Deep-Sea Research, Vol. 35, No. 8, pp. 1335–1354, 1988.
Printed in Great Britain.

0198–0149/88 $3.00 + 0.00
Pergamon Press plc.

On the velocity field of the East Greenland Current

ARNE FOLDVIK,* KNUT AAGAARD† and TOR TØRRESEN*

(*Received* 21 *September* 1987; *in revised form* 25 *February* 1988; *accepted* 4 *March* 1988)

Abstract—Year-long moored measurements from the East Greenland Current near 79°N show its mean southward transport above 700 m to be about 3 Sv and with no obvious seasonal variability. About one-half of this transport appears to be barotropic. There is a rich mesoscale structure in the records, much of which can be interpreted as trains of eddies and eddy-pairs with cross-stream length scales of order 10 km. The lower frequency perturbations typically extend to at least 400 m. Despite the abundance of eddies, their contribution to the heat flux is very small even in the vicinity of the polar front. Local baroclinic instability is therefore not a major source of eddies.

INTRODUCTION

THE southward flux of sea ice with the East Greenland Current (hereafter referred to as the EGC) extends meridionally over some 2500 km, and near its northern end it is estimated to annually carry 4–5000 km^3 of ice equatorward (WADHAMS, 1983; VINJE and FINNEKÅSA, 1986). Only the northward streaming of ice in the western Weddell Sea, along the Antarctic Peninsula, rivals the meridional extent and ice-carrying capacity of the EGC. The importance of the EGC, however, extends beyond its role in influencing the ice distribution, for it is probably also the principal means by which the Arctic Ocean exports the various products of its geochemical and thermodynamic machinery [cf. AAGAARD *et al.* (1985a) for a recent example]. In these matters, as well as in evaluating and modeling the EGC as the western boundary current in a strongly convective wind-driven gyre, we require a knowledge of the velocity field considerably better than is presently the case. It is particularly troublesome that past descriptions of the velocity field have been based largely on dynamic calculations, and then almost exclusively from summer data. Therefore, we effectively have information on neither the low-frequency variability, nor on the barotropic flow field.

The evidence to date suggests that the EGC follows the Greenland continental margin, with the strongest flows overlying the slope [compare AAGAARD and COACHMAN (1968a,b) with PAQUETTE *et al.* (1985)]. Maximum baroclinic currents have typically been computed in the range 20–30 cm s^{-1} in the upper water column over the slope, although recently PAQUETTE *et al.* (1985), using closely spaced stations, found a baroclinic jet with speeds as high as 96 cm s^{-1} near the ice edge. Over the shelf the dynamic topography suggests speeds in the range 5–10 cm s^{-1}. Baroclinic transport estimates vary consider-

* Geophysical Institute, University of Bergen, Allégt. 70, 5007 Bergen, Norway.
† Pacific Marine Environmental Laboratory, National Oceanic and Atmospheric Administration, 7600 Sand Point Way NE, Seattle, WA 98115-0070, U.S.A.

ably, but 2 Sv can be considered characteristic, the majority of which is thought to occur in the upper few hundred meters. However, the few published direct current measurements suggest significant flow at greater depths, and thereby also a net transport which is larger than that indicated by the dynamic heights (AAGAARD and COACHMAN, 1968a).

Except for some recent results on mesoscale features near the ice edge [cf. MIZEX GROUP (1986) for a summary], little is known about the low-frequency variability of the EGC, although there has been speculation about seasonal variability in particular [cf. AAGAARD and COACHMAN (1968a) for a historical review]. If the EGC is the western boundary current of a wind-driven gyre with strong seasonal forcing (AAGAARD, 1970; HANZLICK, 1983), we should expect to see an annual signal, but if the EGC is instead primarily a cog in the thermohaline machinery of the Arctic Ocean (STIGEBRANDT, 1981), there is no obvious reason to expect *a priori* a seasonal variability.

To resolve these and other issues, it became apparent that direct velocity measurements within the EGC were necessary, and in 1984 we began a program to acquire these using moored instrumentation. We here report on the records from the three arrays of three current meters each, moored across the Greenland slope at 79°N during mid-June 1984 to mid-July 1985. Our attention will be directed primarily to the spatial structure of the velocity field and its low-frequency variability, together with their consequences for horizontal fluxes.

METHODS

Currents at the three sites shown in Fig. 1 were measured at hourly intervals with Aanderaa instruments on taut subsurface moorings equipped with acoustic releases. The data have been described in some detail by AAGAARD *et al.* (1985b), and mooring particulars are listed in Table 1. The calibrated data are referred to the center of the sampling time interval (FOLDVIK *et al.*, 1985), and the u- and v-components are,

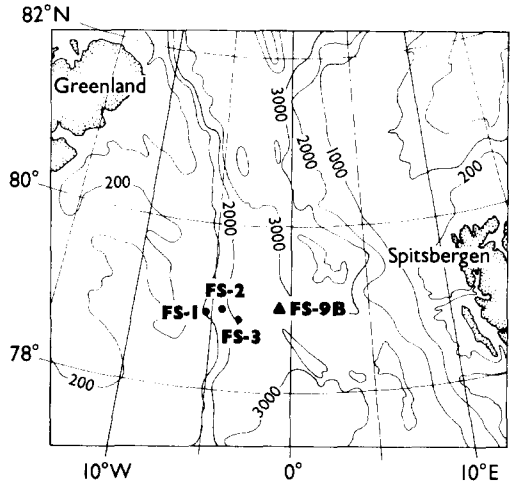

Fig. 1. Mooring locations. Moorings FS-1, -2, and -3 were deployed during 1984–1985, and FS-9B during 1985–1986.

Table 1. *Mooring details. The depths of the two instruments marked by asterisks differ from those given in Table* 2 *of* AAGAARD et al. (1985*b*); *the latter are in error*

Mooring	Instrument number	Nominal depth (m)	Record length (days)
FS-1	3156	94*	396
78°58.7'N, 5°16.1'W	6546	374*	396
1094 m	3161	1069	396
FS-2	6201	78	395
79°00.3'N, 4°25.7'W	3157	378	395
1678 m	3162	1378	273
FS-3	6202	109	394
78°54.9'N, 3°17.7'W	6543	409	394
2359 m	7649	2334	394

respectively, directed east and north. The isobaths in the region are aligned nearly north–south, parallel with the v-axis. In our analysis, the low-pass filtering was done with a four-poled squared Butterworth filter; the coherences were computed according to MOOERS' (1973) method; and the tidal current analysis utilized FOREMAN's (1978) program.

MEAN STRUCTURE

Temperature

The dominant hydrographic feature of the EGC is the Polar Front (hereafter called PF), which separates the cold, low-salinity polar waters west of the front from warmer and more saline water with an Atlantic component to the east. In discussing the temperature field, we find it convenient to follow the water mass nomenclature of SWIFT and AAGAARD (1981), at shallow and intermediate depths taking $T < 0$°C to represent Polar Water (PW), $0 < T < 3$°C Arctic Intermediate Water (AIW), and $T > 3$°C Atlantic Water (AW). [All the deep (>1000 m) instruments measured temperatures below 0°C, corresponding to Greenland or Norwegian Sea Deep Water (GSDW or NSDW), here collectively called Deep Water (DW).]

The position of the shallow (~100 m) and intermediate (~400 m) instruments relative to the mean temperature field across the PF are shown in Fig. 2; the mean temperatures recorded at all nine sites are given in Table 2; and the temperature frequency distributions at each site are shown in Fig. 3. Note that of the instruments in the upper layer, the two westernmost (FS-1 and -2) are embedded in PW essentially the entire time (100 and 97%, respectively), while FS-3 spends only one-half its time in PW and the rest in AIW (40%) and AW (8%), with a maximum observed temperature of 5.2°C. All three intermediate instruments are in AIW the entire time, although there is a pronounced increase in both the temperature and its variance from west to east across the current. The deep instruments show only a very small temperature variance.

Velocity

The magnitude of the v-component in the upper layer (Table 2) is substantially the same at FS-2 and -3, but is significantly less at FS-1, which is located well west of the PF. These direct measurements therefore substantiate earlier conclusions based on dynamic

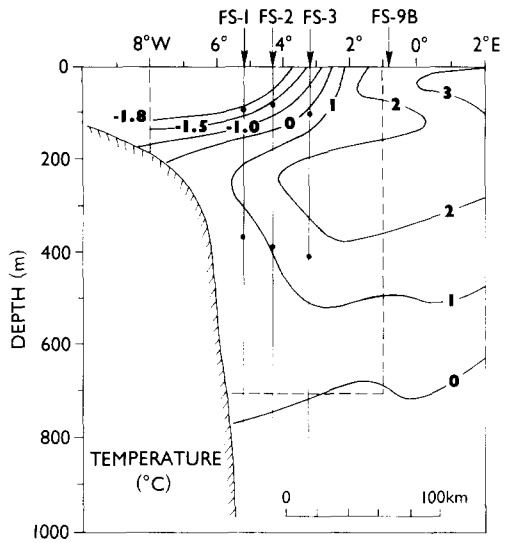

Fig. 2. Composite annual mean temperature section along 79°N.

Table 2. Annual mean temperature and velocities, together with their standard deviations

		u-component mean	*u*-component r.m.s.	*v*-component mean	*v*-component r.m.s.	Speed	Direction (°T)	Temperature (°C)
Upper	FS-1:	0.0	±0.5	–6.2	±0.7	6.2	180	–1.73
	FS-2:	–2.1	±0.5	–8.8	±1.1	9.0	193	–1.45
	FS-3:	–4.1	±0.5	–8.6	±0.9	9.5	205	0.34
Intermediate	FS-1:	–0.1	±0.2	–1.3	±0.3	1.3	184	0.89
	FS-2:	0.0	±0.3	–3.8	±0.5	3.8	180	1.04
	FS-3:	–2.2	±0.3	–5.6	±0.6	6.0	201	1.41
Deep	FS-1:	0.6	±0.1	–2.5	±0.2	2.6	167	–0.22
	FS-2:	0.1	±0.1	–2.3	±0.3	2.3	178	–0.42
	FS-3:	0.2	±0.3	–0.4	±0.9	0.4	153	–0.96

heights and on ice drift that the EGC is swiftest near its eastern edge (KIILERICH, 1945; PAQUETTE *et al.*, 1985; VINJE and FINNEKÅSA, 1986).

Conversely, the magnitude of the *u*-component increases significantly (at the 95% level) from FS-3 to -1, or equivalently, the mean current vector rotates counterclockwise, from 205° through 193°–180°. Therefore the current at FS-1 is nearly parallel with the local isobaths, while that at FS-3 is more nearly aligned with the PF, which in this region is directed about 210° (AAGAARD and COACHMAN, 1968b). The streamlines thus converge, so that the speed must increase downstream, as has been argued previously by AAGAARD and COACHMAN (1968a), MUENCH *et al.* (1986) and VINJE and FINNEKÅSA (1986). A similar streamline convergence is indicated in the intermediate layer between FS-2 and -3.

The vertical shear between the upper and intermediate layers also shows a statistically significant pattern. At FS-1 and -2, the mean shears are identical (1.8×10^{-4} m^{-1}), but at FS-3 the shear is only two-thirds as large. This probably reflects the upper instrument at FS-3 being east of the wedge of PW a large portion of the time, so that the mean density

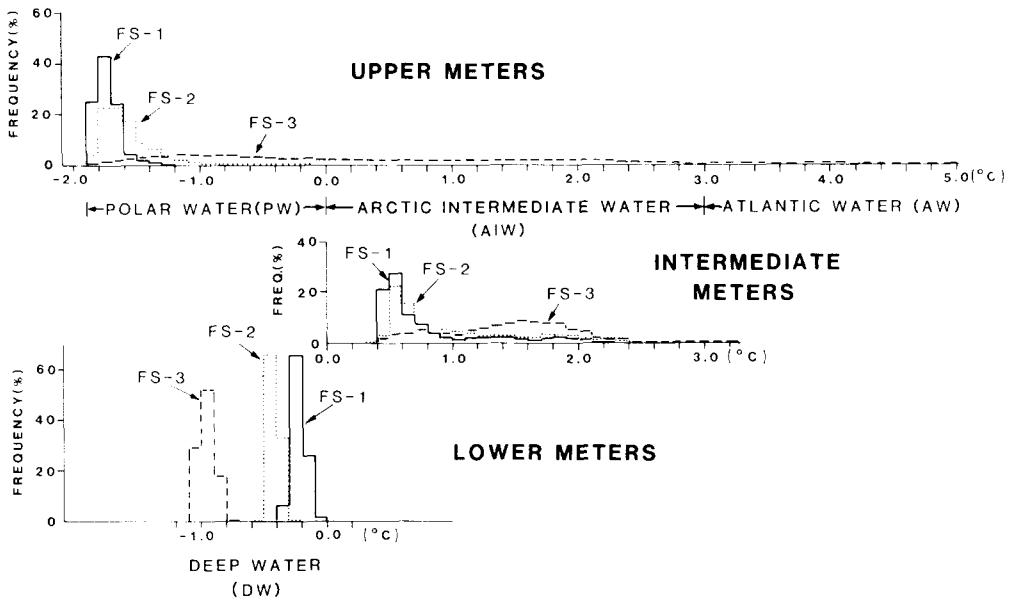

Fig. 3. Temperature frequency distributions from the moored records.

contrast between the upper and intermediate layers is less. A corollary is that over this depth range the horizontal shear increases with depth, so that in the intermediate layer the relative strength of the offshore mean current (near the PF) is even greater than in the upper layer.

Significant mean southward deep flow occurs at both FS-1 and -2, but at FS-3 the much larger fluctuations in velocity lead to a mean current not significantly different from zero. At FS-1 the deep current (25 m above the bottom) has a downslope component, but since the deepest instrument at FS-2 is 300 m above the bottom, we do not know whether a similar downslope motion exists near the bottom there also.

Table 3 shows the mean currents and their standard deviation over consecutive intervals of 3 months. There are substantial differences in temporal behavior at the various instrument sites. In the upper layer, seasonal variations at FS-1 are relatively small, with the difference in 3-month means being only 3.2 cm s^{-1} between the period of maximum flow (October–December) and that of minimum flow (January–March). In contrast, at FS-2 a very strong maximum occurs during the first 3 months (July–September), being over twice the speed at the other two moorings. The current at FS-3 increases almost linearly throughout the year. Inspection of the stick diagrams from August (Fig. 7a) shows that the current at FS-1 and -3 reverses to the north during the first half of the month, but increases substantially southward at FS-2. We interpret these events as resulting from a pair of eddies moving southward with the mean current, one rotating clockwise with its center between FS-1 and -2 and the other rotating counterclockwise with its center between FS-2 and -3. (For a detailed discussion of such eddy events, see the later section on mesoscale motion and coherence.) If we remove this period of eddy passage from the August record and replace it with a constant southward flow of 10 cm s^{-1}, the southward current component for the 3-month period is reduced

Table 3. Three-month mean velocities, together with their standard deviations

		Jul–Aug–Sep		Oct–Nov–Dec		Jan–Feb–Mar		Apr–May–Jun	
u-Component									
Upper	FS-1:	–0.5	±1.1	1.0	±0.8	–0.3	±1.1	–0.4	±0.9
	FS-2:	–3.3	±1.2	–2.0	±0.9	–1.7	±1.1	–1.6	±0.7
	FS-3:	–3.3	±1.3	–3.6	±1.2	–3.6	±0.8	–5.5	±1.0
Intermediate	FS-1:	–0.2	±0.7	0.2	±0.3	0.5	±0.2	–0.6	±0.4
	FS-2:	–0.1	±0.5	–0.0	±0.6	0.2	±0.5	0.6	±0.5
	FS-3:	–1.6	±0.7	–2.1	±0.7	–2.1	±0.7	–2.4	±0.8
Deep	FS-1:	0.8	±0.1	0.7	±0.1	0.8	±0.1	0.3	±0.1
	FS-2:	0.2	±0.2	0.2	±0.1				
	FS-3:	0.6	±0.6	0.4	±0.6	0.0	±0.7	0.2	±0.8
v-Component									
Upper	FS-1:	–7.0	±1.7	–7.6	±1.6	–4.4	±1.5	–6.5	±1.2
	FS-2:	–15.1	±2.3	–8.3	±1.4	–6.4	±2.0	–6.9	±1.9
	FS-3:	–6.1	±2.1	–7.5	±1.3	–9.0	±1.6	–11.2	±2.0
Intermediate	FS-1:	–1.6	±0.9	–2.0	±0.5	–1.6	±0.4	0.0	±0.8
	FS-2:	–6.0	±1.0	–4.7	±1.0	–2.1	±0.9	–2.5	±1.1
	FS-3:	–3.9	±1.2	–5.1	±0.8	–6.2	±1.2	–6.4	±1.6
Deep	FS-1:	–3.5	±0.3	–2.3	±0.3	–2.4	±0.3	–1.8	±0.3
	FS-2:	–2.9	±0.5	–2.3	±0.5				
	FS-3:	1.4	±1.4	–1.1	±1.7	–0.1	±1.5	–1.3	±2.0

from 15 to 13 cm s^{-1} at FS-2, increased from 7 to 8 cm s^{-1} at FS-1, and increased from 6 to 10 cm s^{-1} at FS-3. Thus, while the effect of such eddies on the cross-stream flow is negligible, they can substantially effect the downstream mean value over intervals of months. (Over periods of a year or more, however, eddy effects are small unless a number of eddies with the same rotation consistently pass on one side of the mooring.) While mesoscale motion makes it difficult to distinguish seasonal variations in the flow of the EGC, inspection of the entire records with a view toward eddy contamination suggests that the maximum current lies close to FS-2 during late summer and autumn 1984, but migrates eastward toward FS-3 during the following winter and spring. We note, however, that the vertical shear between the upper and intermediate layers does not follow a similar pattern, for while by far the largest shear is found the first 3 months at FS-2, corresponding to the highest upper-layer speeds, the largest subsequent shear does not migrate toward FS-3, but remains at the western moorings.

At the intermediate instruments the pattern of variability in the 3-month records is on the whole similar to that at the upper ones, whereas in the deep water there are few similarities to the upper and intermediate records.

In summary, our measurements show that over most of the continental slope, there is significant barotropic flow, with the deepest currents in the range 2–3 cm s^{-1} as an annual mean. In at least the upper 400 m the strongest current is normally found near the PF, which at 79°N lies over the foot of the slope. There is considerable lateral structure in the flow at spatial scales of order 20 km or less (our mooring separation varied from 18 to 24 km), at least some of which is associated with eddy or other mesoscale motion. At this latitude, the speed of the EGC increases downstream. While no clear pattern of annual variability emerges from these measurements, they show that large variability does occur

at time scales at least as long as the seasonal. The measurements also point to large mesoscale contamination of the low-frequency bands.

TRANSPORT

While there is considerable interest in the transport of the EGC, the computation of transport is not straightforward, due both to the low-frequency variability of the flow and to the spatially sparse observational net. Nonetheless, we shall make an estimate of volume transport and transport temperature for each water mass by independently constructing mean fields of velocity and temperature in a section at 79°N.

The mean temperature field (Fig. 2) was constructed from a composite of individual sections from the *Edisto* in 1964 (CODISPOTI, 1968), the *Edisto* in 1965 and the *Northwind* in 1981 (PAQUETTE *et al.*, 1985), and the *Lance* in 1984 (RUDELS, personal communication). The isotherm pattern was then adjusted to agree with the mean temperatures observed at the three moorings, and also with that from a fourth mooring near 1°W during 1985–1986 (mooring FS-9B, Fig. 1, unpublished data). Obviously, any individual section may differ significantly from this adjusted composite section.

The field of mean v-component of velocity (Fig. 4) was principally constructed from the current meter averages. These data were extrapolated upward using summer drifting buoy data (SANDVEN, personal communication) to yield the typical velocity profile shown in Fig. 5. The portion of the profile above 100 m is of course only a summer snapshot, and we have no information about its representativeness for other times. However, even if there were no shear above 50 m, the transport velocity above 700 m would change by no more than 15%. Based on the unpublished current measurements near 1°W during 1985–1986, we chose that meridian as the eastern boundary for the southward flow, while the western boundary was set at 8°W. Much of the flow farther west appears to participate in a semi-permanent clockwise gyre (RIIS-CARSTENSEN, 1938; KIILERICH, 1945;

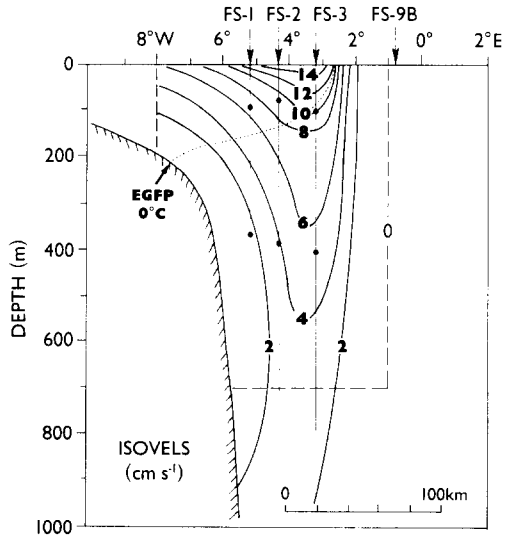

Fig. 4. Annual mean southward velocity across 79°N.

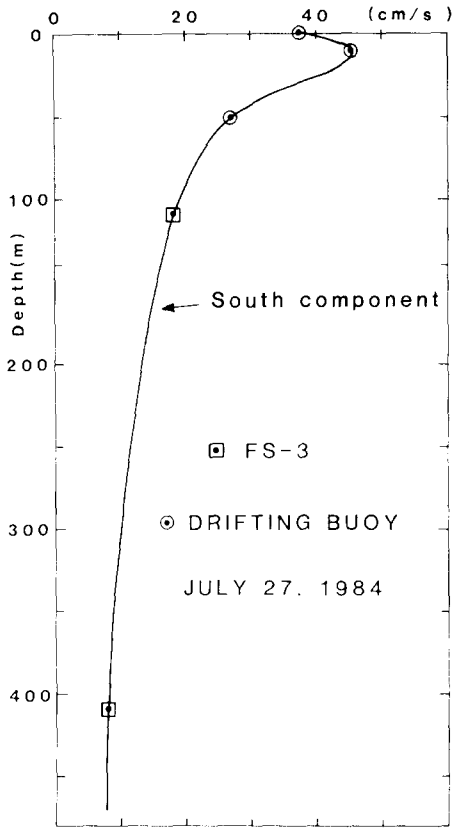

Fig. 5. Typical composite velocity profile for site FS-3 near the Polar Front.

PALFREY, 1967; NEWTON, 1983; VINJE and FINNEKÅSA, 1986), and if so this flow would not contribute significantly to the net southward transport across 79°N. Nevertheless, the possibility remains that we may have underestimated the transport through this assumption. The lower boundary for the transport integration was taken as 700 m, which approximates the lower 0°C isotherm, and thereby the lower boundary of the AIW. Our transport estimates are shown in Table 4, together with the earlier results of AAGAARD and GREISMAN (1975).

This earlier work had assumed a zero net flow through Fram Strait, with the East Greenland and West Spitsbergen currents each transporting 7.1 Sv, but in opposite directions. Our present volume transport estimate for PW is less than 60% of that of Aagaard and Greisman, although as stated we may have underestimated the flux of this water mass. On the other hand, our transport estimate of AW plus AIW, essentially all of which should be expected to occur east of 8°W, is less than 40% of that of Aagaard and Greisman. However, HANZLICK's (1983) estimate of the West Spitsbergen Current (WSC) transport across 79°N of 5.6 Sv during 1976–1977 (and only slightly less the following 2 years) may more nearly complement our present calculation. In particular, Hanzlick found that of his 5.6 Sv total, 3.7 Sv occurred above 600 m. Comparison with Table 4 therefore suggests that the flows above 600–700 m over the Spitsbergen and

Table 4. Volume transport and transport temperature for the East Greenland Current calculated from our data, compared with those from AAGAARD *and* GREISMAN (1975)

	Volume transport (Sv)	Transport temperature (°C)
This study		
PW	−1.0	−1.49
AW + AIW	−2.0	1.29
Total	−3.0	
AAGAARD and GREISMAN (1975)		
PW	−1.8	−1.24
AW + AIW	−5.3	0.52
Total	−7.1	

Greenland continental slopes compensate each other to within about 1 Sv. Whether there in fact is a near-zero net flow through Fram Strait in its entirety, as has frequently been assumed (e.g. MOSBY, 1962; AAGAARD and GREISMAN, 1975), can not be determined from the present data. However, we note that even if the upper flows through Fram Strait fully compensate each other, those below 700 m may not do so, since the deep Arctic Ocean has recently been shown to be renewed from the adjacent shelves (AAGAARD *et al.*, 1985a), so that there is a net conversion of surface to deep waters. This process would then drive a net deep outflow through Fram Strait, continuity being provided by a surface inflow through the Barents Sea, for example. Indeed, we can say very little quantitatively at this point about the exchange of deep water through Fram Strait, other than that it is almost certainly not negligible. For example, the annual mean transport between only 700 and 1000 m through our short section appears to be in the neighborhood of 0.5 Sv.

Compared to the estimates of AAGAARD and GREISMAN (1975), our estimates of transport temperature are very high for AW and AIW and somewhat low for PW (Table 4). The former reflects the pronounced recirculation of AW and AIW initially carried northward with the WSC. Our more extreme transport temperatures, particularly for AW and AIW, suggest that our correspondingly low volume transport estimates will not greatly change the EGC contributions to the overall Arctic Ocean heat budget postulated by AAGAARD and GREISMAN (1975).

MESOSCALE MOTION

The role of mesoscale eddies has been a central issue in recent studies in the Greenland Sea, particularly near the ice edge [cf. MIZEX GROUP (1986) for a summary]. For example, major interest attaches to the extent to which such eddies may control the flux of heat across the PF and thereby influence the ice distribution. Conversely, one might ask whether such eddies play a role in the cross-frontal flux of polar characteristics into the interior Greenland Sea gyre.

Inspection of the low-passed current meter records from FS-1 to -3 suggests an abundance of eddy-like structures with time scales from a few days to several weeks. To illustrate, consider first the time series signatures of the two conceptualized eddies shown

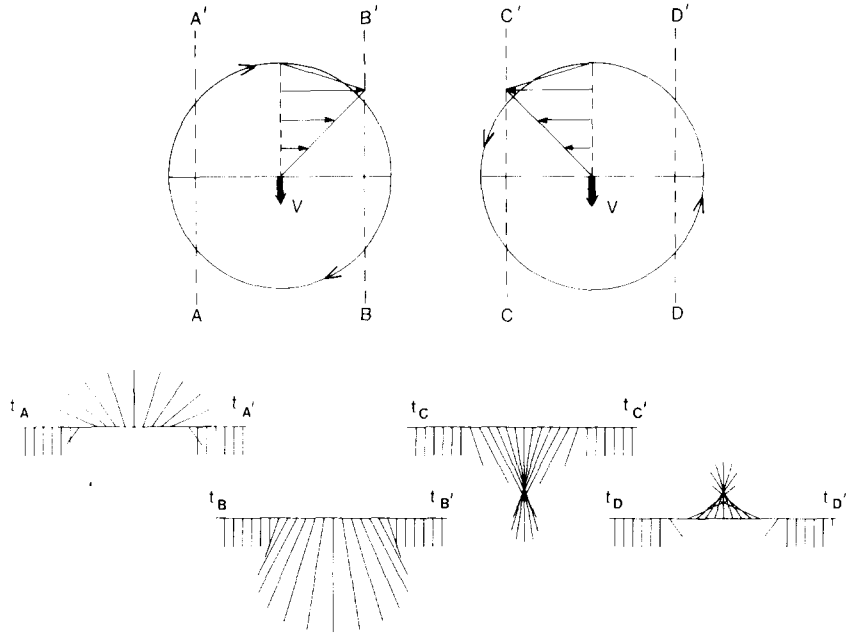

Fig. 6. Conceptualized current records resulting from the passage of eddies.

in Fig. 6, one clockwise (CW) and the other counterclockwise (CCW), being advected with constant velocity past observation points A–D. The resultant time series at the latter locations depend in detail upon the relative strength of the eddies and the ambient velocity field, as well as on the velocity distribution within the eddies. For example, if the tangential velocity were less than the ambient field (in contrast to the situation portrayed in Fig. 6), then the observed velocity time series would not reverse. However, regardless of these details, the registration of all CW eddies will be characterized by open and diverging stick diagrams whereas CCW eddies produce converging vector patterns. An example from a 35-day period beginning in late July is shown in Fig. 7a. Note that while there is some diminution of the signal at the intermediate meters, the vertical correlation is very good, so that this particular disturbance extends well below 400 m. Furthermore, comparison of Figs 6 and 7a suggests that the record segments of Fig. 7a are shaped by a pair of eddies being advected southward past the arrays. In particular, a CW eddy appears to be passing with its center between FS-1 and -2, and a CCW eddy between FS-2 and -3. The lack of a clearly open or closed pattern at FS-2 suggests that the record there is influenced by both eddies.

In addition to advection by the mean velocity field, it is likely that such an eddy pair would create its own net southward advection

$$v' = k/(4\pi a),$$

where k is the vortex strength and $2a$ is the separation of the vortex centers (LAMB, 1932, p. 222). For eddy pairs to pass the moorings as suggested by Fig. 7a, the distance $2a$ must be ~20 km. Figure 7a also suggests a characteristic tangential velocity in the eddies of

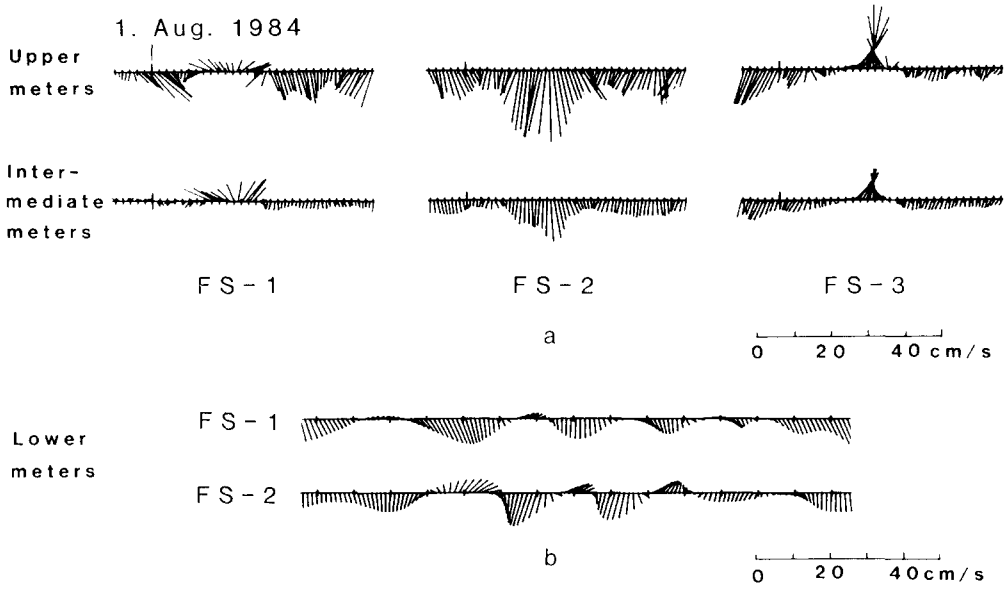

Fig. 7. (a) Thirty-five day extracts from the current records at the upper and intermediate instruments (daily time ticks). Compare Fig. 6. (b) Fourteen-day extracts from the current records at the deep instruments at FS-1 and -2 (daily time ticks beginning 30 June) showing wave-like disturbances.

$\sim$15 cm s^{-1}, so that $k \sim 10^8$ cm s^{-1} and $v' \sim 8$ cm s^{-1}. The latter is comparable to the mean velocity field.

To examine the nature of the mesoscale eddy field and its possible importance, based on the total data set, we first calculate the spatial and frequency characteristics of the eddy kinetic energy. We next attempt to reconstruct the eddy field from coherence computations. Finally, we calculate the eddy heat fluxes over a range of frequencies.

In passing, we note that in addition to eddies, disturbances of a more wave-like nature are also frequent occurrences in the current records, particularly at the lower instruments. An example is given in Fig. 7b, where the oppositely phased signals might represent, say, second-mode shelf waves. We shall consider such disturbances further in the coherence section.

Kinetic energy

We have computed the kinetic energy density for the mean (KM) and the fluctuating (KF) flow components in a number of frequency bands according to

$$\mathrm{KM} = \tfrac{1}{2}(\bar{u}^2 + \bar{v}^2)$$

and

$$\mathrm{KF} = \tfrac{1}{2}\overline{[(u - \bar{u})^2 + (v - \bar{v})^2]},$$

where the overbars denote record-length arithmetic means. The calculation was done by low-passing the data and using successively longer cutoff periods, except for the total fluctuating energy, which was computed without filtering. The results are shown in Table 5.

Table 5. Kinetic energy density for the mean (KM) and the fluctuating (KF) flow components for selected frequency bands

		2–35 h	35 h–4 d	4–15 d	15–30 d	>30 d	Total fluctuating	Mean	Mean + fluctuating
Upper	FS-1:	34.6	7.1	13.8	8.6	8.2	72.3	19.5	91.8
	FS-2:	23.4	5.1	12.2	6.5	14.1	61.3	41.1	102.4
	FS-3:	10.7	6.2	16.9	10. 7	14.6	58.6	45.5	104.1
Intermediate	FS-1:	4.1	0.6	2.7	1.0	2.2	10.6	0.9	11.5
	FS-2:	3.7	1.0	4.4	1.8	2.8	13.7	7.1	20.8
	FS-3:	4.2	3.0	9.9	4.9	4.8	26.8	17.9	44.7
Deep	FS-1:	4.0	0.4	0.9	0.2	0.5	6.5	3.3	9.8
	FS-2:	2.6	1.1	1.9	0.4	0.6	6.6	2.6	9.2
	FS-3:	3.8	6.6	21.0	4.7	8.1	44.2	0.1	44.3

At every instrument KF exceeds KM, with the upper layer being the most energetic. At subtidal frequencies the distributions of KF are similar at FS-1 and -2, with a very large decrease from the upper to the intermediate layer, and then a lesser decrease into the DW. In contrast, while the subtidal portion of KF in the upper layer at FS-3 is comparable to that at the two western moorings, the vertical pattern is entirely different. It decreases far less going into the intermediate layer, and it then increases going into the DW, so that below the upper instruments, KF is very much larger at FS-3 than farther west. The overall impression is of a mesoscale activity which, at the two moorings wholly contained within the EGC, is concentrated in the upper layer. In contrast, at the eastern site such activity not only extends deeper, but is dramatically amplified closer to the sea floor. The details of this mesoscale activity, and the extent to which it represents eddies, waves, or meanders, will be explored in subsequent sections.

With respect to the tidal band energies listed in Table 5, the barotropic components appear to be uniform horizontally over the slope, but the baroclinic tidal currents, which are quite large in the upper layer, increase dramatically approaching the shelf break from the east.

Coherence

Consider first a regular train of eddies or of eddy pairs being advected past an array of observation points (Fig. 8). The advection occurs at rate v and the separation between eddies of similar rotation is l. The times series from points A and A′ will show a current rotating CW (negative rotation) with frequency $\sigma = v/l$, while those from points B and B′ will show CCW (positive) rotation with the same frequency.

Following convention, we refer to the rotary coherence between time series with the same sense of rotation as the inner coherence and to that with the opposite sense as the outer coherence. We assign the coherence to the frequency axis with the same sign as that of the rotation at the easternmost (lower) of the two sites being compared. We calculate the phase relative to the western (upper) site, and for the phase of the outer coherence we do so at the time the phase of the CW component is zero. In Fig. 8 the time series A and A′ will show inner coherence ($C_A - C_{A'}$) at the frequency $-\sigma = v/l$, corresponding to negative rotation at A′, while series B and B′ will show inner coherence ($CC_B - CC_{B'}$) at the same positive frequency, corresponding to positive

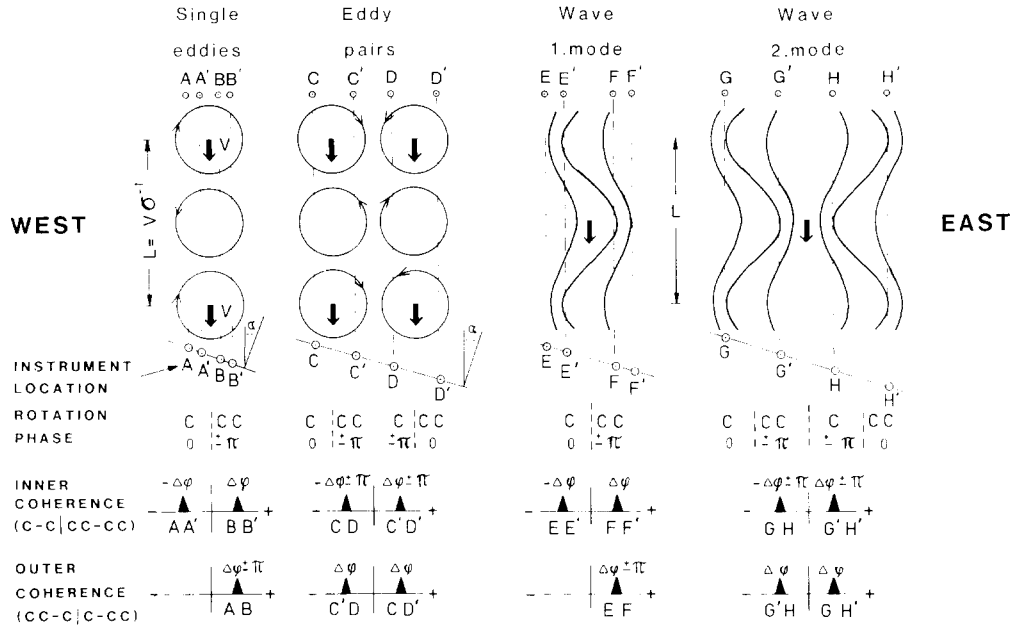

Fig. 8. Conceptualized coherence spectra resulting from the passage of eddies and waves.

rotation at B′. In both cases the rotation will be in phase (zero lag), disregarding for the moment the effect of the station line not being normal to the direction of propagation of the eddies. Similarly, series A and B will show outer coherence ($C_A - CC_B$) on the positive frequency axis, corresponding to positive rotation at site B. The series will be out of phase. For a train of single eddies there will be no outer coherence on the negative frequency axis, since the sign of the rotation at the easternmost site will always be positive. For a train of eddy pairs (Fig. 8) there will in general be four sets of non-zero rotary coherences at frequency σ, each 180° out of phase with the reference series. Figure 8 also shows the expected coherence and phase for first and second mode waves. In particular, we note that on the basis of coherence and phase, in general we cannot distinguish between eddies and waves.

If the trajectory of the eddy train is not normal to the base line between the observation sites, or if one eddy of a pair lags behind the other, then an additional phase lag is introduced. Figure 9 shows this to be

$$\Delta\phi_1 = 360\,\frac{x}{l} = 360\,\frac{\sigma d}{v}\sin\alpha$$

for the case of single eddies, and

$$\Delta\phi_2 = 360\,\frac{x+y}{l} = 360\,\frac{\sigma}{v}\,(d\sin\alpha + l\sin\beta)$$

for a train of eddy pairs. Note that the phase lag is positive when the approach angle is positive, and that it is directly proportional to the frequency and inversely to the

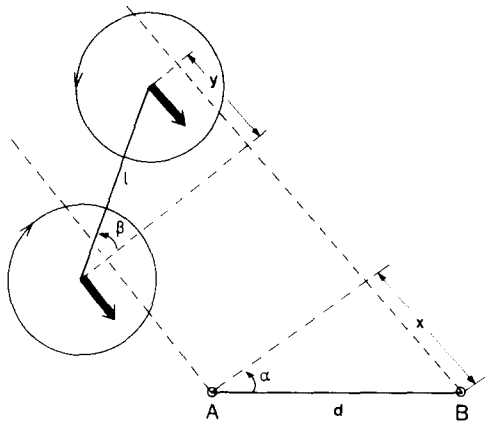

Fig. 9. Generalized geometry of eddy pairs approaching a mooring section.

advection. If we take α, $\beta < 30°$, and, following the earlier example using Fig. 7a, $v \sim 10$ cm s^{-1}, $d \sim 10$ km, and $l \sim 20$ km, then $\Delta\phi_1 < 100°$ and $\Delta\phi_2 < 300°$ for $\sigma = 0.02$ cph (2-day repeatability), and $\Delta\phi_1 < 25°$ and $\Delta\phi_2 < 75°$ for $\sigma = 0.005$ cph (8-day repeatability). Taken together, these considerations suggest that for a non-normal approach we may be able to distinguish between trains of single eddies and eddy pairs on the basis of the substantially different phase relations.

Figures 10 and 11 show the inner and outer coherences, respectively, calculated for the year-long record lengths; only those significant at the 99% level have been included. Both in the PW and in the AIW there is a strong positive low-frequency (>16 days) peak in the outer coherence between FS-1 and -2, but none in the inner coherence; the phase lag is about 165°. This is precisely the signal we would expect from a train of single eddies (or first mode waves) which extends into the intermediate layer and passes with the eddy centers between FS-1 and -2 (compare AB in Fig. 8), possibly with a westerly component of propagation across the mooring base line. The strong vertical inner coherence at identical absolute frequencies (but with opposite sign) supports this interpretation: negative frequency at FS-1 and positive frequency at FS-2. Such eddies would have zero outer vertical coherence, as observed, since the vector rotation is the same at both levels at a given mooring. The phase differences suggest an inclination of the rotational axes of the eddies upward to the north (compare Fig. 8), i.e. opposite to what would be expected from the shearing effect of the mean flow. We note also that there is significant inner vertical coherence at the same low negative frequency at FS-2. We infer from this that similar eddies also pass to the east of FS-2, and in fact the current record portions shown in Fig. 7a illustrate such a situation. Furthermore, the outer positive low-frequency coherence in the upper layer between FS-2 and -3, and the zero inner coherence, which is similar to that calculated for FS-1/FS-2, also speaks to the presence of such eddies. However, there is not a corresponding significant coherence in the AIW between FS-2 and -3, suggesting that the eddies closer to the PF do not extend as deeply. The very high vertical inner coherence at FS-3 therefore must be due to events other than deep-reaching eddies, e.g. to meanderings of the PF or to waves of higher vertical mode. This is also the suggestion of the non-zero vertical outer coherence between the upper and

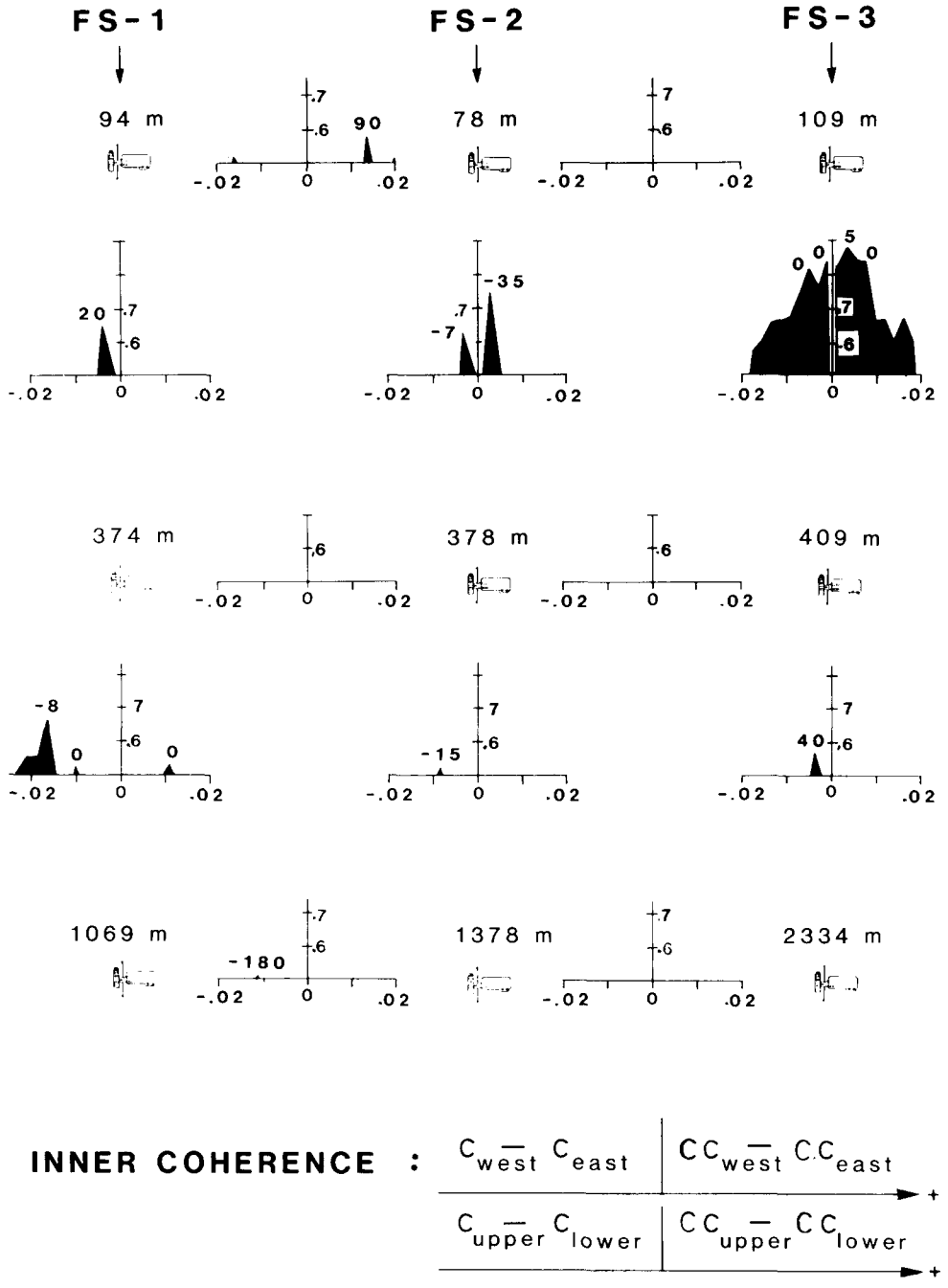

Fig. 10. Horizontal and vertical inner rotary coherence between all adjacent mooring pairs based on the year-long records. The phase in degrees is given above each coherence peak. Only coherences significant at the 99% level are shown.

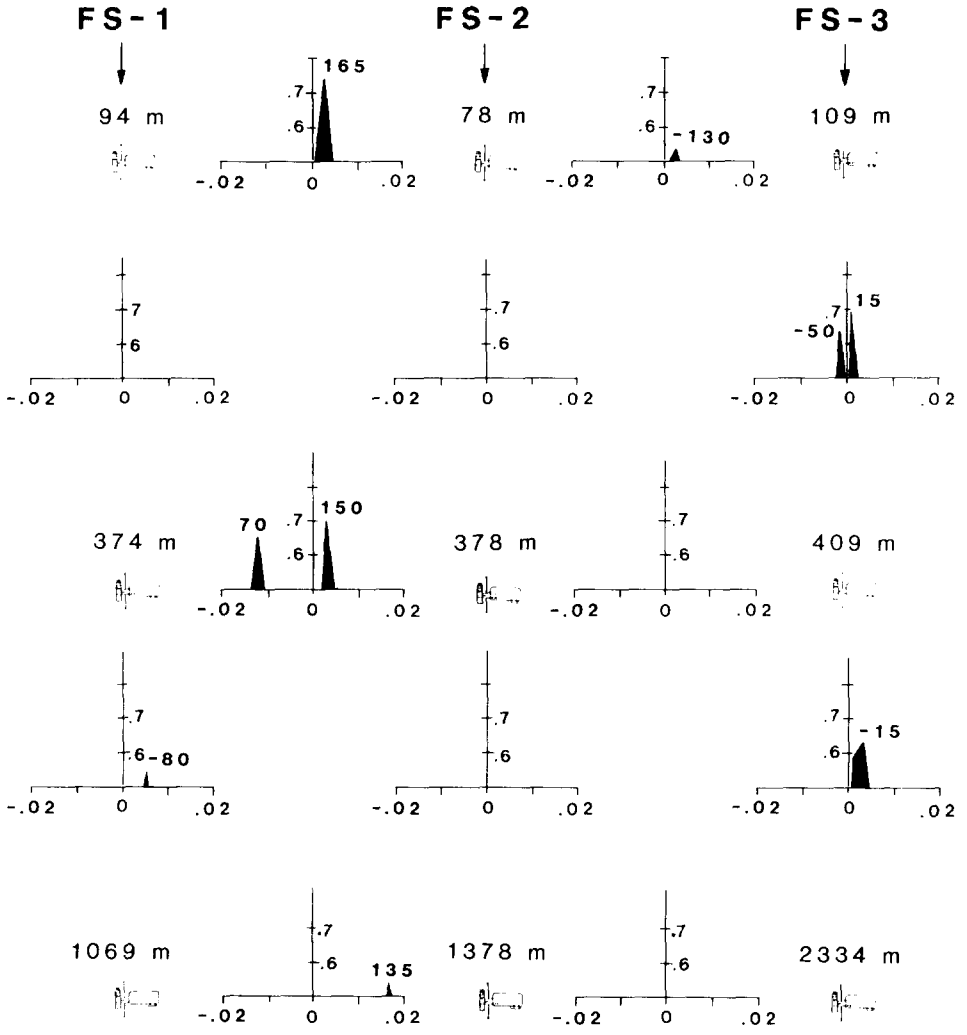

Fig. 11. Horizontal and vertical outer rotary coherence between all adjacent mooring pairs based on the year-long records. The phase in degrees is given above each coherence peak. Only coherences significant at the 99% level are shown.

intermediate layers at FS-3, which from eddies alone would be zero. Finally, we note that for these various low-frequency events (~0.002 cph), an advection of ~10 cm s^{-1} implies an upstream eddy separation $l \sim 180$ km. However, since we have found eddies passing between the moorings, thereby suggesting an eddy size of order 10 km, we infer that in an average sense, the successive eddy pairs are rather widely separated from each other.

Figures 10 and 11 also show significant horizontal coherence between FS-1 and -2 at a time scale of about 3 days. Taken together, the coherence and phase spectra at mid-depth suggest that trains of eddy pairs (or second mode waves) pass moorings FS-1 and -2 directed toward approximately 120°. For the PW the interpretation is more ambiguous and may involve trains of either single or paired eddies (or the corresponding waves). In contrast to the very low-frequency eddies, however, these disturbances do not normally penetrate into the intermediate layer.

Finally, there are several inner and outer coherent frequencies between the DW and the AIW. These probably result from wave-like motions, including ones of higher vertical mode, that extend over a large part of the water column.

Turbulent heat fluxes

In assessing the importance of the eddy field, a critical question is the extent to which it promotes horizontal fluxes, particularly across the PF, but also meridionally. We have therefore calculated record-length zonal and meridional turbulent heat fluxes

$$Q_{Hu} = \rho c_p \overline{(u - \bar{u})\,(\theta - \bar{\theta})}$$

and

$$Q_{Hv} = \rho c_p \overline{(v - \bar{v})\,(\theta - \bar{\theta})},$$

where ρ is the density, c_p the specific heat at constant pressure, and θ the temperature. The calculations were done in the same manner as for the kinetic energy distributions to give the individual contributions of the various frequency bands.

At only three of the nine instruments is the turbulent heat flux significant (Table 6), and in each case the principal contributing frequency band is the lowest (>30 days), in contrast to the turbulent kinetic energy density distribution (Table 5), for which the largest values occur at higher frequencies. With the additional information from the coherence calculations, which suggest that eddies are principally represented by frequencies higher than this, we can infer that, on the whole, temperature anomalies carried by eddies do not contribute significantly to heat flux in the EGC.

Considering Table 6 in more detail, by far the largest turbulent heat flux is the meridional component at the upper instrument at FS-3, where it is directed northward. This results from an asymmetry in the velocity distribution across the PF. More specifically, we showed earlier that this instrument spends about one-half its time in PW and the other in AW/AIW. Therefore the positive turbulent flux means that the speed is higher on the cold (PW) side of the PF than on the warm side. A separation of the velocity record from the upper current meters at FS-3 into cold ($\theta < 0$°C) and warm ($\theta > 0$°C) domains, shows that the mean speed in the former is 10.7 cm s^{-1}, but only 8.3 cm s^{-1} in the latter.

The other statistically significant turbulent heat fluxes occur either at moorings FS-1, farthest removed from the PF, or in the DW below 2000 m. Particularly noteworthy is

Table 6. Record-length turbulent heat fluxes in kW m^{-2} *for selected frequency bands. Fluxes marked by an asterisk are significant at the 95% level*

		2–35 h	35 h–4 d	4–15 d	15–30 d	>30 d	No filter
u-Component							
Upper	FS-1:	0.1	0.5	0.8	1.1	–0.4	2.1
	FS-2:	–0.5	0.9	1.1	–8.0	–14.4	–20.9
	FS-3:	–1.7	–2.4	–10.8	–1.5	32.2	15.8
Intermediate	FS-1:	0.0	0.5	–2.1	–4.6	–8.2	–14.5*
	FS-2:	0.0	–0.9	–1.5	–1.8	0.2	–4.1
	FS-3:	0.0	–0.4	–1.9	–2.5	0.2	–4.6
Deep	FS-1:	0.1	0.0	0.0	0.0	0.2	0.3
	FS-2:	0.0	0.0	0.2	0.0	0.0	0.2
	FS-3:	0.0	0.1	0.2	–0.5	–1.1	–1.4*
v-Component							
Upper	FS-1:	0.1.	–0.2	0.5	1.5	–1.8	0.0
	FS-2:	1.1	–1.1	0.7	3.3	–24.4	–20.5
	FS-3:	–1.0	2.6	–4.6	32.4	72.1	101.4*
Intermediate	FS-1:	0.4	0.1	3.4	2.5	16.8	23.3*
	FS-2:	0.2	1.5	0.3	–0.6	0.7	2.1
	FS-3:	0.5	1.2	8.2	0.3	4.8	14.9
Deep	FS-1:	–0.1	0.0	0.2	0.1	–0.1	0.1
	FS-2:	–0.1	0.0	0.2	0.1	0.5	0.6
	FS-3:	0.0	–0.1	–1.2	–1.0	–2.5	–4.9*

the absence of significant zonal turbulent heat flux near the PF. We return to this matter in the next section.

DISCUSSION

It is apparent from these measurements that barotropic motions are important in the EGC, with significant motion over the slope extending to near-bottom. This means that the EGC is not simply a buoyancy-driven outflow from the Arctic Ocean (contrast WADHAMS *et al.*, 1979), but must also have other driving. To explain the above discrepancy, we probably have to invoke wind forcing in some form, but as a practical matter, from the present data we cannot assess with any confidence the relative importance of the wind-driven circulation and that of the thermohaline forcing associated with either the freshwater flux or with the formation of dense waters in the Arctic Ocean. The matter of large-scale forcing therefore remains an important problem.

A separate issue is the role of eddies in the EGC. While eddies have been a focal point for investigations in the EGC over the past several years, our results suggest that their impact on fluxes is small, at least in the northern portion of the current. In fact, only at the westernmost mooring, far removed from the PF, is there a statistically significant zonal turbulent heat flux (except for at the deep instrument near the bottom of the continental slope). Therefore, unless heat-transporting eddies are confined to lie above the level of our shallowest instruments (78 and 109 m at the two easternmost moorings), it is hard to credit the importance of mesoscale eddies in the cross-frontal fluxes in this

area. A specific point of dynamic importance is that the smallness of the lateral turbulent heat flux implies that the great many eddies which are obviously present are not generated locally through baroclinic instability.

The smallness of the turbulent fluxes also brings to the fore the critical question of how, or indeed if, the EGC interacts significantly with the interior of the Greenland Sea gyre. This question cuts both ways, i.e. does the gyre control events in the EGC to any extent, and does the EGC influence processes in the gyre? For example, if low-salinity water from the EGC is an important control on winter convection in the gyre, where the background stratification is small and major water mass modification is thought to occur, then how and where is the inflow of low-salinity water accomplished (if indeed it is)? It may be a matter of episodic events in the Ekman layer, or of eastward recirculation downstream, or even of cross-frontal eddy fluxes farther south.

Acknowledgements—We greatly appreciate C. Darnall's highly competent mooring work and the fine efforts at sea of the crew of the R.V. *Polarstern*. Our work was supported by the Norwegian Research Council for Science and the Humanities through research grant D.11.10.045 and by the Office of Naval Research through contract N00014-84-C-0111. NOAA Pacific Marine Environmental Laboratory contribution 987.

REFERENCES

AAGAARD K. (1970) Wind-driven transports in the Greenland and Norwegian seas. *Deep-Sea Research*, **17**, 281–291.

AAGAARD K. and L. K. COACHMAN (1968a) The East Greenland Current north of Denmark Strait, 1. *Arctic*, **21**, 181–200.

AAGAARD K. and L. K. COACHMAN (1968b) The East Greenland Current north of Denmark Strait, 2. *Arctic*, **21**, 267–290.

AAGAARD K. and P. GREISMAN (1975) Toward new mass and heat budgets for the Arctic Ocean. *Journal of Geophysical Research*, **80**, 3821–3827.

AAGAARD K., J. H. SWIFT and E. C. CARMACK (1985a) Thermohaline circulation in the arctic Mediterranean seas. *Journal of Geophysical Research*, **90**, 4833–4846.

AAGAARD K., C. DARNALL, A. FOLDVIK and T. TØRRESEN (1985b) Fram Strait current measurements 1984–1985. University of Bergen Rep. 63 and University of Washington Rep. M85-9, 85 pp.

CODISPOTI L. A. (1968) Some results of an oceanographic survey in the northern Greenland Sea, summer 1964. U.S. Naval Oceanographic Office Technical Rep. TR-202, 49 pp.

FOLDVIK A., T. KVINGE and T. TØRRESEN (1985) Bottom currents near the continental shelf break in the Weddell Sea. In: *Oceanology of the Antarctic Continental Shelf, Antarctic Research Series*, **43**, pp. 21–34.

FOREMAN M. G. G. (1978) Manual for tidal current analysis and prediction. Institute of Ocean Sciences Pacific Marine Science Rep. 78-6. 70 pp.

HANZLICK D. J. (1983) The West Spitsbergen Current: transport, forcing, and variability. Ph.D. Dissertation, University of Washington, 127 pp.

KIILERICH A. B. (1945) On the hydrography of the Greenland Sea. *Meddelser om Grønland*, **144**, 63 pp.

LAMB H. (1932) *Hydrodynamics*, 6th edn, Cambridge University Press, 738 pp.

MIZEX GROUP (1986) MIZEX East 83/84: the summer marginal ice zone program in the Fram Strait/Greenland Sea. *EOS*, **67**, 513–517.

MOOERS C. N. K. (1973) A technique for the cross spectrum analysis of pairs of complex-valued time series, with emphasis on properties of polarized components and rotational invariants. *Deep-Sea Research*, **20**, 1129–1141.

MOSBY H. (1962) Water, salt, and heat balance of the North Polar Sea and of the Norwegian Sea. *Geofysiske Publikasjoner*, **24**, 289–313.

MUENCH R. D., G. S. E. LAGERLOEF and J. T. GUNN (1986) 1984–85 current observations in the East Greenland Current: a preliminary description. *MIZEX Bulletin*, **7**, 41–53.

NEWTON J. L. (1983) Hydrographic structure over the northeast Greenland shelf. In: *The physical and chemical oceanography of the Arctic Ocean*, Oceanographic Institute, University of Gothenburg Special Rep. 1, p. 22.

PALFREY K. M. Jr (1967) Physical oceanography of the northern part of the Greenland Sea in the summer of 1964. M.S. thesis, University of Washington, 63 pp.

PAQUETTE R. G., R. H. BOURKE, J. F. NEWTON and W. F. PERDUE (1985) The East Greenland Polar Front in autumn. *Journal of Geophysical Research*, **90**, 4866–4882.

RIIS-CARSTENSEN E. (1938) Fremsaettelse af et dynamisk-topografisk kort over Østgrønlandsstrømmen mellem 74° og 79° N. Br. paa grundlag af hidtidig gjorte undersøgelser i disse egne. *Geografisk Tiddsskrift*, **41**, 25–51.

STIGEBRANDT A. (1981) A model for the thickness and salinity of the upper layer in the Arctic Ocean and the relationship between the ice thickness and some external parameters. *Journal of Physical Oceanography*, **11**, 1407–1422.

SWIFT J. H. and K. AAGAARD (1981) Seasonal transitions and water mass formation in the Iceland and Greenland seas. *Deep-Sea Research*, **28**, 1107–1129.

VINJE T. and Ø. FINNEKÅSA (1986) The ice transport through the Fram Strait. *Norsk Polarinstitutt Skrifter*, **186**, 39 pp.

WADHAMS P. (1983) Sea ice thickness distribution in Fram Strait. *Nature*, **305**, 108–111.

WADHAMS P., A. E. GILL and P. F. LINDEN (1979) Transects by submarine of the East Greenland Polar Front. *Deep-Sea Research*, **26**, 1311–1327.